Tree Physiology 43, 501–514
https://doi.org/10.1093/treephys/tpac132

Methods paper

Use of near-infrared spectroscopy to estimate physical, anatomical and hydraulic properties of *Eucalyptus* wood

Antonio José Barotto[1,9], Alejandro Martínez-Meier[2,3], Vincent Segura[4], Silvia Monteoliva[5], Jean-Paul Charpentier[6], Javier Gyenge[3,7], Anne Sophie Sergent[3,8], Frédéric Millier[6], Philippe Rozenberg[3,6] and María Elena Fernández[3,7]

[1]Cátedra de Dendrología, Facultad de Ciencias Agrarias y Forestales, Universidad Nacional de La Plata, CC 31 (1900) La Plata, Argentina; [2]INTA EEA Bariloche, Grupo de Ecología Forestal, UEDD IFAB INTA-CONICET - Laboratorio de Ecología, Ecofisiología y Madera (LEEMA), Modesta Victoria 4450 (8400), Río Negro, Argentina; [3]Laboratorio Internacional Asociado LIA-Forestia (INTA - INRAE - UNAH); [4]UMR AGAP Institut, Univ Montpellier, CIRAD, INRAE, Institut Agro, F-34398 Montpellier, France; [5]INFIVE UNLP-CONICET, Diag. 113 esq. 61 (1900), La Plata, Argentina; [6]UMR 0588 BioForA, INRAE, ONF, Orléans, France, 2163 Avenue de la Pomme de Pin, CS 40001 Ardon, 45075 Orléans Cedex 2, France; [7]Grupo Forestal, UEDD IPADS INTA-CONICET-Oficina Tandil, Rodríguez 370 (7000), Tandil, Argentina; [8]Consejo Nacional de Investigaciones Científicas y Técnicas (CONICET), Argentina UEDD IFAB INTA-CONICET - Laboratorio de Ecología, Ecofisiología y Madera (LEEMA), Modesta Victoria 4450 (8400), RíoNegro, Argentina; [9]Corresponding author (jose.barotto@agro.unlp.edu.ar)

Received May 12, 2022; accepted November 11, 2022; handling Editor Sebastian Pfautsch

Tree breeding programs and wood industries require simple, time- and cost-effective techniques to process large volumes of samples. In recent decades, near-infrared spectroscopy (NIRS) has been acknowledged as one of the most powerful techniques for wood analysis, making it the most used tool for high-throughput phenotyping. Previous studies have shown that a significant number of anatomical, physical, chemical and mechanical wood properties can be estimated through NIRS, both for angiosperm and gymnosperm species. However, the ability of this technique to predict functional traits related to drought resistance has been poorly explored, especially in angiosperm species. This is particularly relevant since determining xylem hydraulic properties by conventional techniques is complex and time-consuming, clearly limiting its use in studies and applications that demand large amounts of samples. In this study, we measured several wood anatomical and hydraulic traits and collected NIR spectra in branches of two *Eucalyptus* L'Hér species. We developed NIRS calibration models and discussed their ability to accurately predict the studied traits. The models generated allowed us to adequately calibrate the reference traits, with high R^2 ($\geq$0.75) for traits such as P_{12}, P_{88}, the slope of the vulnerability curves to xylem embolism or the fiber wall fraction, and with lower R^2 (0.39–0.52) for P_{50}, maximum hydraulic conductivity or frequency of ray parenchyma. We found that certain wavenumbers improve models' calibration, with those in the range of 4000–5500 cm^{-1} predicting the highest number of both anatomical and functional traits. We concluded that the use of NIRS allows calibrating models with potential predictive value not only for wood structural and chemical variables but also for anatomical and functional traits related to drought resistance in wood types with complex structure as eucalypts. These results are promising in light of the required knowledge about species and genotypes adaptability to global climatic change.

Keywords: hydraulic efficiency, NIRS, resistance to embolism, wood anatomy, wood density.

Introduction

Tree breeding programs and wood industries require simple, time- and cost-effective techniques to process large volumes of samples typical of their usual activities and protocols (Viana et al. 2009, Alves et al. 2012, Luss et al. 2015, Tsuchikawa and Kobori 2015). Particularly, in tree breeding, non-destructive sampling is desirable, since it allows the conservation of genotypes for future research (Schimleck et al. 1999). Techniques such as those using X-ray, high-frequency (Polge 1966, Jacquin et al. 2017) or neutron methodology (Mannes et al. 2007) allow to describe wood physical properties such as wood density at high spatial resolution within wood samples (i.e., microdensity profiles). In this regard, the characterization of wood physical properties using microdensity profiles has advanced substantially since it is now possible to scan and obtain the digitalized image quickly. Alternatively (or complementary) to those techniques, in recent decades, near-infrared spectroscopy (NIRS) technology has been acknowledged as one of the most powerful techniques for wood analysis (Alves et al. 2012, Inagaki et al. 2012), making it the most used tool for high-throughput phenotyping in tree breeding programs (Hein 2012). NIRS is a particular type of vibrational spectroscopy, which is based on the study of responses to electromagnetic radiation in the frequency range between 12,820 and 4000 cm^{-1} or 780 and 2500 nm.

As in other materials, NIR spectra taken in wood contain information regarding its chemical composition and molecular structure, which ultimately determine its particular properties (Schwanninger et al. 2011). Some of the NIRS advantages, for its use in wood industry and forestry research, are the high speed of spectra acquisition, the varied range of samples from which spectra can be taken, with little or no preparation (Schwanninger et al. 2011), and the possibility of extending its predictive capacity to standing trees, through the development of new portable devices. However, information obtained by this method cannot be directly interpreted (Luss et al. 2015) but requires the use of mathematical analysis techniques and multivariate statistics. Partial least squares regression (PLS-R) models are typically used to develop calibrations that relate the NIR spectra with properties assessed by conventional reference methods (Viana et al. 2009, Hein 2012, Leblon et al. 2013, Luss et al. 2015). Then, the calibrations can be used to predict the properties of other samples (Hein 2012).

The NIRS technique can be considered as an alternative to explore jointly wood physical properties and other wood characters, such as those related to its chemical composition, or even hydraulic properties. Conventional measurements of chemical properties and of wood hydraulic properties are commonly carried out through slow, laborious and often expensive methods, generally applicable to a limited number of samples. Previous studies have shown that a significant number of anatomical, physical, chemical and mechanical wood properties can be estimated through NIRS, for both angiosperm and gymnosperm species (e.g., Schimleck and Evans 2004, Viana et al. 2009, Alves et al. 2012, Luss et al. 2015, Tsuchikawa and Kobori 2015). These studies are mainly focused on wood properties related to specific industrial uses (e.g., moisture content, wood density, physical and mechanical properties, chemical composition, etc.). Indeed, these properties, in addition to growth rate and bole form, have been traditionally the main selection targets in tree breeding programs. However, in a global climate change scenario, tree breeders face the challenge of developing new selection criteria based not only on wood quality traits but also on functional traits with an adaptive value, such as those related to resistance to environmental stress (Booth 2013, Lachenbruch and Mcculloh 2014).

Xylem hydraulic properties (such as maximum specific hydraulic conductivity and resistance to embolism) play a key role in survival against extreme climatic events (Anderegg et al. 2016, Choat et al. 2018), interacting in a complex way with other physiological traits and environmental conditions (Adams et al. 2017, Hajek et al. 2022). These properties derive from wood anatomical characteristics, such as xylem conduits diameter, the grouping and connectivity among conduits (vessels or tracheids), and the size, number and ultrastructure of intervascular pits, among others (Hacke et al. 2006, 2009). In turn, these anatomical and functional characteristics may be correlated with other properties such as wood density. At the interspecific level, a higher wood density is related to an increase in embolism resistance by xylem tension (Hacke et al. 2001, Jacobsen et al. 2005), affecting the response to climate and increasing drought resistance, but in different degree and form depending on the biome and type of drought (Greenwood et al. 2017, Serra-Maluquer et al. 2022). However, at the intraspecific level—at which breeding programs operate—this relationship does not always hold: the correlation between wood density and resistance to embolism can have different signs and magnitudes (Cochard et al. 2007, Corcuera et al. 2011, Dalla-Salda et al. 2011, Barotto et al. 2018). Beyond the different relationships between wood density and embolism resistance, the intraspecific variability in this last trait seems to be rather limited between populations of several species (*Pinus* spp.: Lamy et al. 2014, López et al. 2016; *Fagus sylvatica*: Wortemann et al. 2011; *Quercus petraea*: Lobo et al. 2018; *Austrocedrus chilensis*: Gyenge et al. 2005), with a few examples that have described significant differences between populations of humid versus xeric sites (e.g., *Quercus ilex*: Peguero-Pina et al. 2014; *Eucalyptus obliqua*: Pritzkow et al. 2020). More studies are certainly needed at this level of organization, exploring not only the genetic variability but also the plasticity in this adaptive trait (and others) in response to changing environmental conditions, a topic much less studied (e.g., Grossiord et al. 2017). However, exploring the variability of hydraulic traits by conventional techniques is complex and

time-consuming (5–30 samples/day, depending on the applied technique), clearly limiting its use in breeding programs and studies demanding large amounts of samples. Thus, techniques facilitating the measurement of resistance to embolism would be of very high scientific and applied interest.

To the best of our knowledge, only two studies have reported NIRS calibrations for wood hydraulic properties such as resistance to embolism (Luss et al. 2015, Sergent et al. 2020), both of which have been carried out in gymnosperm species (*Picea abies* and *Austrocedrus chilensis*, respectively). Another study used mid-infrared (MIR) spectra to predict wood density and resistance to embolism in angiosperms at the interspecific level (Savi et al. 2019). Therefore, there is still a gap in knowledge about how well NIRS can describe anatomical and functional traits for most woody species and particularly for a genus with great commercial importance like *Eucalyptus* L'Hér.

Eucalyptus spp. wood exhibits particular characteristics, presenting diffuse porosity, with large-diameter solitary vessels surrounded by vasicentric tracheids and vasicentric paratracheal axial parenchyma (e.g., Barotto et al. 2016). The great variety of environments in which eucalypts develop, added to the particular characteristics of their wood, results in a broad range of wood densities (InsideWood 2004–onwards). This is one of the most relevant wood properties that can be estimated by NIRS, commonly evaluated in tree breeding programs (Schimleck et al. 1999, Alves et al. 2012, Inagaki et al. 2012). Demonstrated by our own works (Barotto et al. 2016, 2018), in this genus wood density is often related to wood hydraulic traits and, consequently, with the species ecological fitness, being an integrating characteristic of the different cell types that are involved in water transport through the xylem (Barotto et al. 2017). However, these relationships are not straightforward, so it is not known a priori if NIRS would be able to describe wood anatomy and function in eucalypts with reasonable precision for its use in high-throughput scanning at the intraspecific level or within the range of values given by close-related taxa. In this framework, we explored the ability of NIRS for the prediction of anatomical, physical and hydraulic wood properties in two closely related species of this genus: *E. globulus* Labill. and *E. viminalis* Labill. The analyzed samples came from these species breeding programs. Therefore, their genetic origin is known, and it was possible to select the samples in order to maximize the intraspecific phenotypic variation for the studied traits.

Materials and methods

Site and plant material

This study was carried out using plant material from two provenance/progeny tests (half-sib families) of two *Eucalyptus* species, of the Forest Genetic Improvement Program trial network of the National Institute of Agricultural Technology (INTA) of Argentina: *E. globulus* and *E. viminalis*. The trial corresponding to *E. globulus* consists of 250 progenies and includes 12 native Australian provenances, as well as provenances previously introduced in Portugal, Spain, Chile and Argentina. This trial is located in Balcarce city, Argentina (37° 45′ S, 58° 17′ W, 97 m above sea level) and was planted in 1995 (Lopez et al. 2001). The climate in this region, according to the Köppen climate classification, is oceanic (Cfb). The mean annual temperature is 13.3 °C and the average annual precipitation is about 800 mm (climate-data.org, Balcarce city, Argentina). The *E. viminalis* trial is composed of 77 provenances. It was planted in October 2000 (Cappa et al. 2010) near the town of Del Valle, Argentina (35 51′ S, 60° 43′ W, 63 m above sea level). According to the Köppen classification, the climate of this region corresponds to humid subtropical climate without dry season (Cfa), with a mean annual temperature of 15.8 °C and an average annual precipitation of ∼970 mm (climate-data.org; Del Valle city, Argentina). In fact, both trials share quite similar environments in the studied region.

Sample selection, collection and processing

Measures of Pilodyn® on standing trees allowed identifying high and low wood density families corresponding to high and low wood density provenances in each species. Within each selected family, some trees were randomly selected and branch sample was collected. In this sense, we assume to cover the entire range of wood density, maximizing intraspecific variability (Table 1). It is important to note that initial Pilodyn® measures—which were used only for the selection of families for further determinations—were carried out at stem level, while hydraulic and anatomical traits, as well as wood density, were measured on the branches collected on the selected trees. The methods of measurement of hydraulic traits are destructive and impose the use of branches when the trees cannot be felled, which was the case here. The branches were sampled in consecutive years, during the first days of February (2015 for *E. globulus* and 2016 for *E. viminalis*), in the morning and during a period of high soil water availability to minimize water stress. Between one and three branches were extracted from the basal portion of each tree crown. In *E. globulus*, six to eight trees from two families were selected from two provenances. In total, 32 branches were sampled: 15 from high and 17 from low wood density provenances. For *E. viminalis*, eight trees from three and two families were selected in the high and low wood density provenances, respectively, according to the number of living trees at the sampling time. In total, 34 branches were obtained: 16 from high and 18 from low wood density provenances. The branches were 3–6 mm in diameter and more than 1 m long. Once the branches were obtained, they were re-cut under water, wrapped with wet rags and stored in black polyethylene bags to avoid dehydration. It is important to note that the sampling, including more than one branch from each tree, has the primary objective of covering the largest possible variation of each trait

Table 1. Species, provenances, families, number of individuals (and branches) sampled, mean Pilodyn® penetration value (PILO) and relative classification of provenances as high or low stem wood density.

Species	Provenance	Latitude	Longitude	Family	*n*	PILO (mm)	Classification
Eucalyptus globulus	Jeeralang, Victoria	38° 20′ S	146° 31′ E	1	4 (10)	9.75	High density
				2	2 (5)	10.25	
	Parker Spur, Victoria	38° 47′ S	143° 35′ E	61	4 (11)	12.12	Low density
				63	4 (6)	11.75	
Eucalyptus viminalis	Errinundra Road, Victoria	37° 26′ S	148° 52′ E	84	2 (3)	9.08	High density
	Bald Hills, Victoria	37° 12′ S	148° 11′ E	27	3 (6)	9.13	
				25	3 (7)	10.00	
	Federation Road, Victoria	37° 28′ S	146° 00′ E	118	6 (14)	11.79	Low density
	Bonang, Victoria	37° 16′ S	148° 44′ E	55	2 (2)	11.38	

in our model system, irrespective of the source of that variation (the individual, the provenance or the species).

A previous study (Barotto et al. 2016) has shown that branch segments longer than 30 cm produce adequate vulnerability curves to xylem embolism in these species. Hence 30 cm was chosen as the minimum length to develop the vulnerability curves. Branches were re-cut and debarked under water to their final length and stored during a maximum of 2 weeks in distilled water with 1% sodium hypochlorite at 4 °C (Jinagool et al. 2015) to avoid the development of microbial activity.

Reference properties assessment

Hydraulic variables Embolism resistance was estimated from vulnerability curves, developed by the air injection method, according to the following protocols:

(i) Perfusion during 15 min at 1 Bar pressure to remove any initial embolism.
(ii) Xylem maximum hydraulic conductivity measurement (ks max) with the pipette method (Sperry et al. 1988).
(iii) Constant pressure applied within the embolism chamber for 2 min (from −0.5 to −6.5 MPa).
(iv) Stabilization until constant ks (no bubbles coming out from the branch extremes).
(v) ks measurement.

Steps (i) and (ii) were performed only at the beginning of each curve, whereas steps (iii) to (v) were repeated for each point of the embolism curve (one complete curve per branch). These curves were developed using a Scholander-type pressure chamber (model 10, BioControl, Buenos Aires, Argentina) with a embolism chamber attached to it (Figure 1A). The percentage loss of hydraulic conductivity (PLC) was estimated from the ks losses for every applied pressure level in relation to the maximum ks (ks max) of each branch. Once the vulnerability curve was completed, the cumulative density function (CDF) of Weibull distribution was fitted to it:

$$PLC/100 = 1 - \exp\left[-\left(T/b\right)^{c}\right]$$

where T is the tension (considered as equal in absolute value to the positive pressure applied in the embolism chamber), b is the Weibull scale parameter and c is the Weibull shape parameter. Usual parameters like P_{50}, P_{12} and P_{88} (i.e., water potential inducing 50%, 12% and 88% losses of hydraulic conductivity, respectively; MPa) and the slope between P_{12} and P_{88} of each vulnerability curve (which denotes how fast conductivity is lost) were estimated from this model.

Anatomical variables Once vulnerability curves to xylem embolism were obtained, branches were adequately conditioned to obtain the histological sections for anatomical measurements. The central portion of the branches, corresponding to the location of the embolism chamber, was removed and cross-sections were cut using a sliding microtome (20–25 μm thick; Figure 1B). Histological sections were mounted in water without staining process. The following variables were measured in transverse sections: vessel diameter (VD, μm), vessel frequency (VF, mm^{-2}), halo area (Ha, μm^2), fiber wall fraction (FWF, %) and ray frequency (RF, mm^{-1}). The Ha is a variable defined in Barotto et al. (2016) for these species, which integrates the cells surrounding a solitary vessel, including vasicentric tracheids, fiber tracheids and axial parenchyma. These cell types cannot be identified in transverse section but are quantified in conjunction. As an integrating variable of wood anatomy, wood basic density (BD, g cm^{-3}) was calculated in the two remaining branch segments (Figure 1C), as oven-dry mass (at 103 °C) per unit of fully saturated wood volume. For more detailed information about how the variables were measured and their functional significance, see Barotto et al. (2016) and Barotto et al. (2018).

NIRS acquisition

Samples were stored inside a stabilization chamber under controlled conditions of temperature and humidity (21 °C and 60%, respectively) before spectral measurements, to guarantee

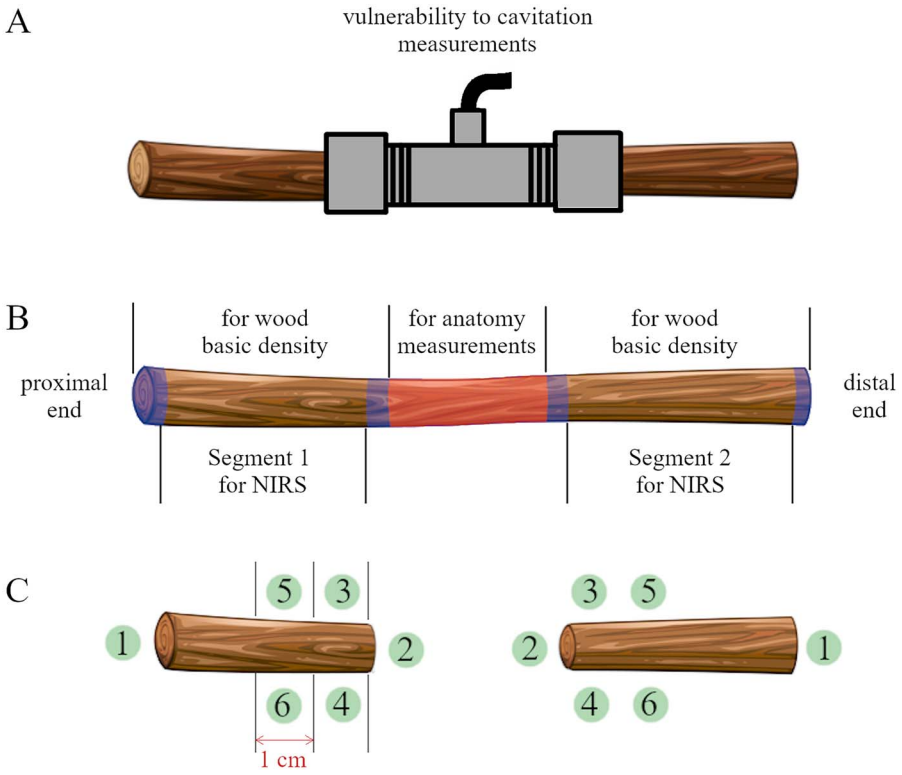

Figure 1. Scheme of the procedure followed to obtain reference measurements (vulnerability to embolism, anatomy and wood basic density) and NIRS spectra in branches. Numbers 1–6 refers to the position and order of NIR spectra acquisition in each branch segment.

sample uniform conditions. Spectra were collected with a Fourier transform spectrophotometer (PerkinElmer Spectrum 400; Waltham, MA, USA) using the NIRA module (integrating sphere) in diffuse reflectance mode, within the range of 10,000–4000 cm^{-1}. The spectral resolution was 8 cm^{-1} and there was a zero-filling factor of 4, resulting in absorbance values every 2 cm^{-1}. Each spectrum consisted of 64 averaged scans, and Spectralon® thermoplastic resin was used as a reference. Spectra were taken over a month, under average laboratory conditions of 36.2% relative humidity and 24 °C temperature. A spot of 1 cm in diameter was used for spectra acquisition.

Since the central portion of the branches was removed after hydraulic measurements to determine wood anatomical characteristics, there remained two segments for each branch (Figure 1C): segment 1, corresponding to the portion closest to the insertion in the stem (proximal end), and segment 2, corresponding to the portion closest to the tip of the branch (distal end). The specific protocol for spectra acquisition involved the following steps:

(i) To avoid measuring portions that might have been exposed to oxidation of their constituents, a thin section was removed from the ends of each segment (Figure 1B, blue section).

(ii) Within each segment, spectrum 1 was taken on the transversal section (T) furthest from the center, whereas spectrum 2 was also acquired on the T section but closest to the central portion (Figure 1C).

(iii) Spectra from the longitudinal section (L) were taken starting from the portion closest to the center, taking the spectra 3 and 5 on the side exposed to tension (upper side) and the spectra 4 and 6 on the opposite side. Spectra 3 and 4 were those closest to the center (Figure 1C).

Spectra processing

To correct possible light scattering effects and highlight the differences in light absorption at different wavenumbers, different pre-treatments were systematically applied to raw spectra (RAW): normalization (N), detrend (DT), first and second derivatives (D1 and D2, respectively), and first and second derivatives of normalized spectra (ND1 and ND2, respectively). For D1 and D2, as well as ND1 and ND2, Savitzky–Golay method (Savitzky and Golay 1964) was implemented in the *signal* package (Signal developers 2014) in R software (R Core Team, 2021), with a window size of 74 and 122 cm^{-1} for D1 and D2, respectively. Principal component analysis, by means of *prcomp* and *dudi.pca* functions from *ade4* package in R, was performed on the spectra (transformed or not), in order to explore their variation patterns and to identify possible outliers. In this initial exploratory analysis, no samples were removed as outliers.

Table 2. Anatomical and hydraulic variables, and wood basic density (mean ± standard deviation), carried out in branches of *E. globulus* and *E. viminalis*. *P*-values from analysis of variance (ANOVA) outlined in bold indicate significant differences between species. The coefficient of variation (CV) corresponds to the data set for both species, describing the maximum variation of each trait given by the pooled data used in NIRS calibration models.

Variable	*E. globulus*	*E. viminalis*	CV (%)	*P*-value
VD (μm)	41.89 ± 5.08	39.82 ± 4.39	11.72	0.1144
Ha (μm^2)	2,302 ± 490	4,075 ± 760	33.49	**0.0001**
VF (mm^{-2})	74.41 ± 18.02	50.76 ± 8.46	29.24	**0.0001**
RF (mm^{-1})	23.32 ± 3.89	22.08 ± 2.79	14.78	0.1782
FWF (%)	63.42 ± 6.73	56.96 ± 5.87	11.7	**0.0004**
BD (g cm^{-3})	0.62 ± 0.04	0.55 ± 0.06	10.5	**0.0001**
ks max (kg m^{-1} MPa^{-1} s^{-1})	1.87 ± 1.06	1.7 ± 0.73	50.72	0.4456
P_{12} (MPa)	−1.95 ± 0.98	−1.64 ± 0.47	42.65	0.1106
P_{50} (MPa)	−3.36 ± 1.23	−4.02 ± 0.61	26.93	**0.0073**
P_{88} (MPa)	−4.99 ± 1.63	−7.75 ± 2.95	43.01	**0.0001**
Slope (% MPa^{-1})	29.96 ± 14.6	14.52 ± 4.59	59.86	**0.0001**

Model calibration

In this study, we explored calibration models pooling the data of both *Eucalyptus* species, which—as known from previous studies cited below—do differ in some wood functional and anatomical variables, and do not in others. We believe that our data set is valuable to disentangle the ability of the method to predict traits within a limited range, like the one given by close-related taxa such as those studied. We provide, however, the descriptive information of traits at intraspecific level to discuss later the contribution of both species to the variation of each studied trait.

The initial analysis showed, for certain spectra transformations, different variation patterns by section, making it possible to discern them (Figure 1S available as Supplementary data at *Tree Physiology* Online). Based on these results, interspecific model calibrations were carried out, considering both sections separately and together (T, L and T + L). Calibrations for hydraulic and anatomical variables, as well as for basic wood density, were performed using partial least squares regression or regression on latent structures (PLS-R), using the *pls* package (Mevik and Wehrens 2007) from R software.

The best calibration model for each trait was selected through an ad hoc index, the Model's Fitness Indicator (MFI). This MFI considers the linear relationship between the observed and predicted values (R^2), the number of latent variables (linear combinations of predictive variables that maximize the covariance between X and Y) used by the model (*lv*) and the ratio between the outliers (*out*) and the total number of samples (*n*):

$$\mathrm{MFI} = \left[\frac{((maxlv + 1) - lv)}{maxlv}\right] \cdot R^2 \cdot \left[1 - \left(\frac{out}{n}\right)\right]$$

where *maxlv* is the maximum number of *lv* allowed in the model (10). A cross-validation scheme (4 segments, 40 iterations) was used to compute the coefficient of determination (R^2). The optimal number of factors was determined by the Wold's R criterion (Wold 1978). As suggested by Minasny and McBratney (2013), the RPD (Ratio of Performance to Deviation) is not reported here because it has a direct relationship with R^2 and is, therefore, redundant.

The first component of the MFI equation seeks to penalize those models with a greater number of latent variables. The selection of many latent variables will produce data overfitting and will result in a model that will probably only be suitable for the data from which it was derived (high specificity). The second component enhances the high coefficient of correlation between the observed and predicted values. The objective of the third component of the equation is to penalize those models that removed the largest number of samples. As can be seen from the formula, MFI values varied between 0 and 1, the latter indicating a perfect fit. The use of the MFI allowed us to compare and select the best models in each stage, weight the models obtained in each stage for the same trait, as well as to compare the fit between traits. Finally, the CARS algorithm (Li et al. 2009) was used to the automatic selection of wavenumbers, helping to increase the MFI with a maximum of 500 iterations per pre-treatment.

The amplitude of the variation in the studied traits was estimated by means of the coefficient of variation of each trait and by determining whether there were significant differences between the datasets from the two studied species with ANOVA, without considering the source of variation within each dataset (individual tree or provenance).

Results

Descriptive statistics for the analyzed variables are presented in Table 2. Differences between the data coming from each species were found in 6 of the 11 anatomical and hydraulic

Table 3. Summary of the calibrations for each variable at branch level, obtained through three successive stages. Spectra: longitudinal (L), transversal (T) and a combination of both spectra (L + T). P.p. (pre-processing): no processing (RAW), first derivative (D1), second derivative (D2) and second derivative of normalized spectra (ND2); Stage: calibration stage; *N*: number of samples used; lv: number of latent variables; Outliers: proportion of samples eliminated from the model; Wavenumbers: number and proportion of wavenumbers selected by CARS algorithm; MFI: Model's Fitness Indicator; Ranking: order of the calibrated model based on MFI value.

Variable	Spectra	P.p.	Stage	*N*	lv	R^2	Outliers	Wavenumbers		MFI	Ranking
Ha	L	D2	1	54	1	0.68				0.68	1
			2	46	1	0.81	14.8%			0.69	
			3	46	1	0.82	14.8%	25	0.8%	0.69	
VF	L	D2	1	54	1	0.46				0.46	2
			2	46	1	0.70	14.8%			0.60	
			3	46	1	0.71	14.8%	380	12.7%	0.61	
BD	L + T	ND2	1	66	2	0.54				0.48	3
			2	59	2	0.71	10.6%			0.57	
			3	59	2	0.73	10.6%	283	9.4%	0.59	
FWF	T	ND2	1	54	2	0.25				0.22	4
			2	50	3	0.54	7.4%			0.40	
			3	48	3	0.75	11.1%	69	2.3%	0.53	
Slope	L	D1	1	64	2	0.18				0.16	5
			2	46	2	0.57	28.1%			0.37	
			3	45	2	0.83	29.7%	5	0.2%	0.53	
VD	T	D2	1	54	1	0.02				0.02	6
			2	51	4	0.46	5.6%			0.30	
			3	51	4	0.74	5.6%	409	13.6%	0.49	
P_{88}	L + T	ND2	1	64	2	0.05				0.05	7
			2	45	2	0.59	29.7%			0.37	
			3	46	3	0.80	28.1%	9	0.3%	0.46	
P_{12}	L + T	D1	1	64	1	0.04				0.04	8
			2	49	4	0.57	23.4%			0.31	
			3	50	4	0.75	21.9%	11	0.4%	0.41	
ks	T	ND2	1	66	1	0.02				0.02	9
max			2	55	4	0.51	16.7%			0.30	
			3	55	4	0.52	16.7%	124	4.1%	0.30	
RF	T	RAW	1	54	2	0.01				0.01	10
			2	37	1	0.33	31.5%			0.23	
			3	36	1	0.40	33.3%	3	0.1%	0.27	
P_{50}	L	RAW	1	64	1	0.01				0.01	11
			2	44	2	0.28	31.3%			0.18	
			3	44	2	0.39	31.3%	23	0.8%	0.24	

variables, as well as for BD. No significant differences were observed in the data sets of each species in VD, RF, ks max and P_{12}.

The calibration models for the reference variables (Table 3) show that no unique branch section nor transformation of the raw spectra presented the best fit for all the variables. Four variables were better represented by the T spectra (FWF, VD, ks max, RF), four by the L spectra (Ha, VF, Slope, P_{50}) and the remaining three by the L + T spectra (BD, P_{88}, P_{12}). In turn, two of them presented the better fit for RAW data (RF, P_{50}), two for D1 (slope, P_{12}), three for D2 (Ha, VF, VD) and four variables with ND2 (BD, FWF, P_{88}, ks max).

Due to the penalization criteria imposed on the MFI, none of the models presented more than four latent variables. MFI progressively improved through the successive stages, as a result of the favorable evolution of the goodness-of-fit indicator used for its calculation (R^2). Comparing the calibrations performed in the third stage of analysis (Figure 2), the best-predicted variables were those representing the Ha and VF, followed by the BD, FWF and slope. At the other end, the models with the lowest fitness were those for P_{50} and RF, both of which obtained using the RAW spectra. In the last stage of data analysis, the percentage of outliers detected and eliminated from the model varied between 5.6% for VD and 33.3% for the RF. The selection of wavenumbers with CARS algorithm presented higher specificity for some variables and ranged between 0.1% and 13.6% of the total spectra wavenumbers (Table 3).

In addition to the different number of wavenumbers selected for each trait, there were differences in the location of these wavenumbers along the spectrum (Figure 3). Comparing the

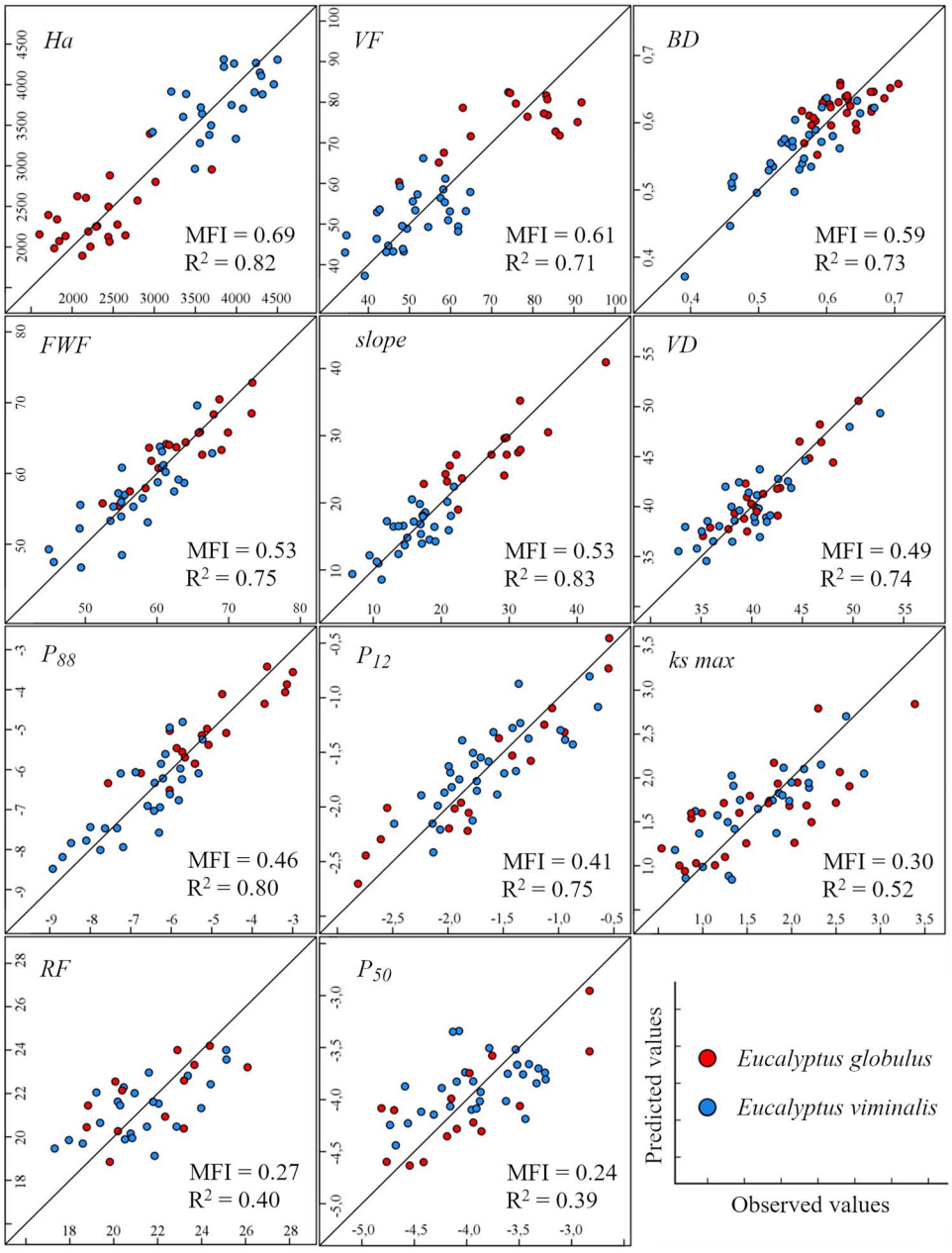

Figure 2. Observed versus expected values from the calibration of predictive models for reference variables at branch level, ordered according to the MFI.

location of selected wavenumbers allows us to observe that, while some spectra portions are involved in predicting more than one variable, there are several portions not related to any trait analyzed. In this sense, the spectrum portion between 5500 and 4000 cm^{-1} showed the highest predictive capability, with at least one selected wavenumber for every considered trait, with some of these wavenumbers contributing to predict up to five variables (4008–4000 cm^{-1}: BD, ks max, VD, VF and Ha). On the contrary, the portion between 10,000 and 5500 cm^{-1} presented wavenumbers that were selected for only six variables (Figure 3).

Basic wood density (BD) and FWF, two variables closely related to cell wall proportion, showed a similar level of fit and fitness index (Figure 2, Table 3) but were defined by different number and location of wavenumbers, although some of them were shared between variables (seven wavenumbers in three portions of the spectra; Figure 3). The hydraulic variables showed a low number of selected wavenumbers, varying between 5 and 23, for slope and P_{50}, respectively. While selected wavenumbers were mostly placed between 5500 and 4000 cm^{-1}, no overlapping among them was recorded. The xylem maximum hydraulic conductivity presented a

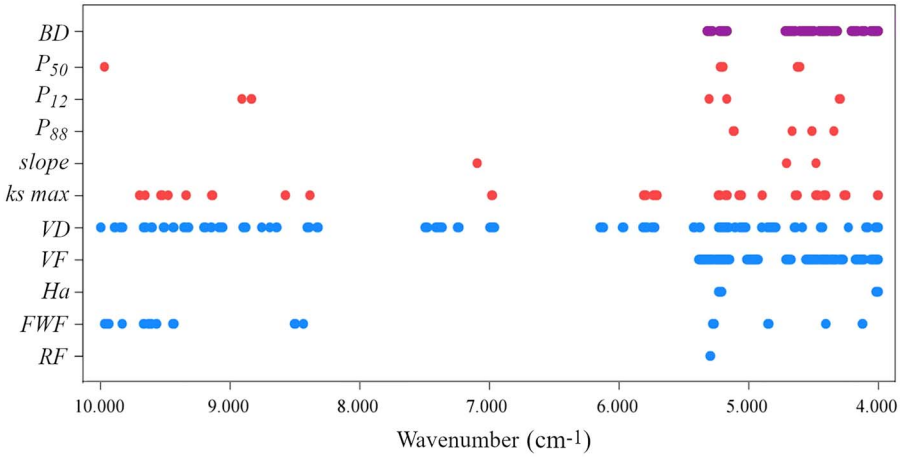

Figure 3. Graphic comparison of spectra wavenumbers selected by CARS algorithm for the modeling of the reference variables at the branch level.

relatively low fit and exhibited a higher number of selected wavenumbers, compared with the other hydraulic variables, sharing few with them (Figure 3). However, we must consider that hydraulic variables were calibrated under different spectra transformations. Closely related to hydraulic variables, VD showed low specificity for wavenumbers selected for its estimation (Figure 3). This anatomical trait was estimated with a high level of fit through 409 wavenumbers, which were distributed homogeneously throughout the spectrum. As expected, derived from the functional relationship between them, the size of the xylem conductive elements and the maximum conductivity shared a considerable number of wavenumbers (54), in several portions (11) of the spectrum. Related to the vessels' size, their frequency (i.e., vessel number per unit of xylem area) was the second variable with the highest number of wavenumbers detected and the second-best calibration (according to the MFI), with a coefficient of determination around 0.71, using a single latent variable. This variable shared a large number of wavenumbers with VD (67) in the spectrum portion between 5500 and 4000 cm^{-1}. Closely related to vessels characteristics, the area occupied by their surrounding cells (quantified by Ha) presented the highest degree of fit of all the variables analyzed, ranking first according to MFI (Table 3). On one hand, it presented a high coefficient of determination, and on the other, it was only defined from a single latent variable, with a low proportion of outliers. Furthermore, the total number of wavenumbers that defined this variable overlapped with those wavenumbers selected for determining VD. Finally, and despite the relatively low performance of the calibration for the RF, this variable was the one that showed the greatest specificity, with only three selected wavenumbers, shared with the VF.

Discussion

Our results, based on a relatively small sample size but a high number of studied anatomical and functional traits, suggest that NIRS can be used to predict different wood traits in a type of angiosperm wood with a complex cell arrangement and composition, such as the *Eucalyptus* wood. The capability of this technique to capture the variation at the studied taxonomic level is particular to each analyzed trait and does not depend on the internal variation of the studied traits given by interspecific, intraspecific or intraindividual differences, which is further discussed in the following paragraphs. The spectrum portion with the highest number of selected wavenumbers was the region between 5500 and 4000 cm^{-1}. This region, which represents the spectrum portion corresponding to the combination bands of the fundamental vibrations, is highly sensitive to structural differences and has a particular spectral signature that resembles the 'fingerprint' region of IR spectroscopy (Beć et al. 2018), with numerous applications (Ozaki 2012). Probably, the increased absorbance in this portion and the appearance of more pronounced peaks and valleys, in comparison with other spectrum regions, reflected in a better way the changes in the reference measurements.

From the methodological point of view, the calibrations performed at the branch level did not result in a single ideal section for the estimation of all the reference variables. In this sense, different anatomical variables were better estimated through spectra taken in transverse (T), longitudinal (L) or T + L sections. On the other hand, both anatomical and hydraulic reference variables were quantified in a different branch segment than the one used for spectra acquisition. This would indicate that it is possible to estimate wood traits from NIRS spectra taken from a close but different wood portion than that where the reference variable was measured.

Few studies have analyzed the relationship between physical and hydraulic wood properties and the NIRS absorption spectra obtained in branches, and none was found combining also anatomical traits. After an extensive literature review, results were only found for five of the reference variables analyzed in this study: basic wood density, P_{12}, P_{50}, P_{88} and the slope of the vulnerability to embolism curve. Regarding the results

obtained for wood density, the most studied variable through NIRS calibrations, Costa et al. (2018) developed a calibration for 432 species and 1066 samples, using 27 latent variables, without spectra processing, which resulted in a fitted model with a coefficient of determination of 0.76. The level of fit obtained in the present study is somewhat lower (R^2 = 0.73), but it was achieved from only 2 close species, 59 samples and using 2 latent variables, which suggests the high performance of the method to describe the variation in wood density, even within a relatively narrow range of variation. Furthermore, Sergent et al. (2020) carried out two calibrations for this wood trait, with 50 branch samples from *Austrocedrus chilensis* (a gymnosperm), and found a lower level of fit than the present study (R^2 of 0.59 and 0.63).

The estimation of P_{50} from NIRS finds only two antecedents, corresponding to Luss et al. (2015) and Sergent et al. (2020), as indicated before. In the first case, the authors worked with *Picea abies* and employed a similar sample size to that used in this study, but, unlike ours, wood samples were obtained from stem wood and flattened with a sliding microtome to homogenize the wood surfaces. They fitted several models with specific wavenumber selection, using spectra obtained from lateral and transversal sides of stem wood beams. The best-fitted model (R^2 = 0.65) was obtained from the combination of first derivative (1D) and multiplicative scatter correction on the spectra from transversal surfaces, using three latent variables. In the case of Sergent et al. (2020), the *Austrocedrus chilensis* samples were also debarked branches with no additional sample treatment. The two models fitted, one from normalized spectra and the other from the second derivative without wavenumber selection, presented R^2 of 0.6 and 0.54, with an outlier proportion of 20 and 10%, and using three and seven latent variables, respectively. Taking these three factors into account, the overall fit obtained in that study is higher than the one reported here, with a low number of outliers detected. Regarding the aforementioned studies, it is relevant to note that they were carried out in gymnosperm species, which have simpler and more homogeneous wood anatomy than angiosperms in general, and *Eucalyptus* in particular. There is, however, another antecedent (Savi et al. 2019) where the relationship between P_{50} and MIR (mid-infrared) spectra was analyzed, in an interspecific study of 23 angiosperm species, which did not include any *Eucalyptus* species. These authors worked with 90 branch samples and took the spectra in cross-section, obtaining a fitted model with an R^2 of 0.49. Although this level of adjustment is higher than the one found in our study for P_{50}, these authors worked with a wider range of variation in resistance to embolism (−1.19 to −5.36 MPa) and a larger number of samples. We cannot discard either the effect of the methodological procedures applied for the determination of vulnerability to embolism in the different studies since each method (bench-dehydration, centrifuge, air-injection, pneumatic, microtomography) has its own strengths and drawbacks, potentially rendering different curves for similar subjects. In this study, we applied the air-injection method, which gave similar results for the studied species than the pneumatic method (Barigah et al. 2019), but the accuracy of different methods for each particular species needs to be further investigated. On the other hand, as has been concluded in other studies (Barotto et al. 2016, 2018), the relationship between P_{50} and wood anatomical components of *Eucalyptus* species, especially those that determine xylem safety, is especially complex. Regarding this, it is worth saying that the inverse relationship between the size of conductive elements and resistance to embolism observed in many woody species has not been verified in *Eucalyptus* genus (Fernández et al. 2019). If NIRS reflect, in part, the wood anatomical constitution, the low correlation observed in previous works between P_{50} and the anatomical variables (Barotto et al. 2016), added to the reduced number of samples and the null surface preparation of branches, could be responsible for the poor predictive quality of this functional trait.

In contrast to P_{50}, the parameters P_{12} and P_{88} showed a high level of fit, with a coefficient of determination of 0.75 and 0.8, respectively, which are higher than those found for *A. chilensis* (P_{12}: R^2 = 0.6, D1, 7 latent variables, 16% of outliers; P_{88}: R^2 = 0.37, RAW, 3 latent variables, 10% of outliers; both without wavenumber selection; Sergent et al. 2020). These parameters have been significantly related to certain anatomical components and physical characteristics of *Eucalyptus* wood. On one hand, P_{12} has been related to anatomical characteristics such as VD, Ha, VF and hydraulic variables, such as maximum conductivity (ks max) (Barotto et al. 2016). On the other hand, P_{88} has shown significant correlations with fiber wall characteristics and wood density (Barotto et al. 2018). Having found models with a high level of fit for these functional variables is consistent with the highly significant relationships between them and the anatomical variables which, ultimately, determine their hydraulic function. Likewise, these parameters define the slope of the vulnerability to embolism curve, which represents the speed at which the loss of conductivity occurs, as a function of the water potential. The model developed for this functional trait exhibited the highest fit level for all the variables considered (R^2 = 0.83), being much higher than that reported for *A. chilensis* (R^2 = 0.26, RAW, 2 latent variables and 16.5% of outliers; Sergent et al. 2020). Although P_{50} is the most widely used parameter to establish comparisons in resistance to embolism (Jacobsen et al. 2005), the results found seem to indicate a lower functional value of this trait in *Eucalyptus* species, which would be defined by the air entry point (P_{12}) and the speed at which the embolism process develops (slope). Moreover, several studies have found that P_{88} is a key parameter related to drying limits for tree mortality, i.e., the point of no-return, in angiosperm species (Barigah et al. 2013, Urli et al. 2013, Lamacque et al. 2020, Mantova et al. 2021), including

Eucalyptus camaldulensis (Barigah et al. 2021). Therefore, its proper prediction in angiosperms takes special relevance.

The few antecedents assessing anatomical characteristics of wood conductive elements through NIRS were also developed for gymnosperm species by Schimleck and Evans (2004), Schimleck et al. (2004) and Jones et al. (2005). Moreover, Ona et al. (1999) were able to estimate VD from stem samples of two *Eucalyptus* species (*E. globulus* and *E. camaldulensis*) through Raman spectroscopy (another type of vibrational spectroscopy), using two latent variables and getting a lower fit than the one obtained in the present study. In the case of cells surrounding the vessels, made up of variable amounts of axial parenchyma, fiber tracheids and vasicentric tracheids, the only antecedent to this study corresponds to Abe et al. (2013), who evaluated the relationship in the proportion of vascular bundles and parenchyma through NIRS in *Elaeis guineensis* (Oil palm), from ground samples, obtaining a model with a high level of fit. In our study, vessels' size and frequency, as well as the size of accompanying cellular elements, were estimated through NIRS with a considerable level of fit, sharing a variable number of significant wavenumbers. Ray frequency (RF), to our knowledge, has not been previously analyzed and results obtained here allow us to infer that this trait could be quantified by a few key wavenumbers, which are also important to estimate VF. Beyond the fact that wavenumber selection can increase the specificity of the generated models, these results are in line with results previously obtained (Barotto et al. 2016), where a positive and highly significant correlation was observed between the frequency of the vessels and the rays for these species. Considering the traits related to the cell wall characteristics, FWF is an indirect and relative measure of its dimensions, which integrates the cell lumen into it, and is usually significantly related to the BD (Ziemińska et al. 2013). These variables shared only a few significant wavenumbers, which could indicate that, although they are related, they are differentially determined by wood physical and chemical composition. Although there is no previous work that addresses the relationship between wall fraction and NIRS, Viana et al. (2009) established calibrations to predict fiber wall thickness from stem wood of six *Eucalyptus* clones. These authors found high heterogeneity in the results, with correlation coefficients that varied between 0.1 and 0.86, depending on the clone considered. Also, in another angiosperm species, Shukla et al. (2021) calibrated PLS models for fiber morphological parameters (fiber length and diameter, and lumen diameter) from radial and tangential faces of *Tectona grandis* wood samples, obtaining robust models ($R^2 > 0.87$). Furthermore, Schimleck et al. (2004) established regressions to predict tracheid wall thickness from *Pinus taeda* stem wood, in both radial and transverse surfaces, with a coefficient of determination that varied between 0.90 and 0.91, showing a level of fit similar to our study. Finally, Schimleck and Evans (2004) estimated the fiber wall thickness from stem samples of *Pinus radiata* with similar results, obtaining calibrations with R^2 values between 0.88 and 0.91. Although not directly comparable, these results allow us to affirm that wall dimensional characteristics from cellular components that determine the wood structure, such as their thickness or relative proportion, can be adequately estimated through this methodology.

The amplitude of values of the studied traits could be a driver of the goodness of fit of NIRS and any reference variable, besides the biological relationships between wood chemical composition/anatomy with wood function or density. By analyzing this effect in our studied system, it was noticed that the four calibrations with the highest degree of adjustment (Figure 2) were those that also presented highly significant interspecific differences on reference values (Table 2). In the opposite extreme, two of the worst predicted variables (RF and ks max) did not present differences in the datasets coming from the two studied species (Table 2). However, the existence of differences linked to the species origin in a reference variable and the corresponding relatively high degree of trait variation were not determinants per se of high model fitness. In this regard, the model developed for ks max, the variable with the second highest level of variation, presented, as previously mentioned, a low level of fit. On the other hand, the variable with the lowest coefficient of determination (P_{50}) presented significant differences between the datasets of both species, while P_{12} and VD, two variables that did not vary between species, showed a relatively high level of adjustment. In our study, we implicitly expected that having two species would increase the ranges of studied traits compared with the generally limited intraspecific variation, and therefore, more robust models could be developed. However, this assumption was not held, and a high inherent variation of each trait—within or between species—was not a condition to achieve a good model. More studies are needed to decipher the causal relationships between the observed empirical relationships between NIR spectra and the different studied traits.

Conclusions

The results presented in this work are, to our knowledge, the first where an integral view of structural, anatomical and functional variables are analyzed by NIRS, as well as presenting data of two closely related angiosperm species. We have shown that the use of NIRS allows the calibration of models with potential predictive value not only for wood structural and chemical variables with industrial value, a largely studied topic, but also for anatomical and functional traits related to drought resistance in the *Eucalyptus* genus. In this sense, the models generated allowed us to adequately calibrate, with a certain degree of variability, the reference traits evaluated in two temperate *Eucalyptus* species of quite similar wood density. The best-calibrated models were

those for some functional traits (slope of the vulnerability to embolism curve and P_{88}) and anatomical characteristics (Ha). With intermediate fit values, there was also a mixture of physical (BD), functional (P_{12}) and anatomical (VD, VF and FWF) variables. Among the models with the lowest prediction capacity were those developed for some functional traits, such as ks max and P_{50}, and one anatomical trait (RF). It is important to note that the level of fit in the prediction of P_{12}, P_{88} and the slope of the vulnerability curve was higher than for P_{50}, which is consistent with results reported in previous studies showing a lower relationship between the latter and anatomical traits in the studied species. The results of this study indicate that certain spectrum wavenumbers would improve models' calibration. This specificity would reflect the chemical properties of the different wood components which, grouped in diverse anatomical structures, modulate the physical and functional characteristics of wood. Although the results are promising, it is necessary to further investigate if the selected wavenumbers show the same specificity in other species, extending the analysis to other *Eucalyptus* species and to other genera. In this regard, the developed models cannot be extrapolated to other species without specific calibrations. However, we consider that these results open interesting avenues in light of the required knowledge—and methodological tools to acquire it—about species' and genotypes' adaptability in the framework of global climatic change.

Supplementary data

Supplementary data for this article are available at *Tree Physiology* Online.

Funding

This study was funded by the EU H2020-MSCA-RISE-2014 project TOPWOOD (Wood phenotyping tools: properties, functions and quality - 645654).

Data availability

Anatomical, physical, hydraulic and NIRS data that support the findings of this study are available on this link: https://drive.google.com/file/d/1B5tfNmW3jpDKYBX4VFYZiwY2moNjXv32/view?usp=sharing.

References

Abe H, Murat Y, Kubo S et al. (2013) Estimation of the ratio of vascular bundles to parenchyma tissue in oil palm trunks using NIR spectroscopy. Bioresources 8:1573–1581.

Adams HD, Zeppel MJB, Anderegg WRL et al. (2017) A multi-species synthesis of physiological mechanisms in drought-induced tree mortality. Nat Ecol Evol 1:1285–1291.

Alves A, Santos A, Rozenberg P, Pâques LE, Charpentier J-P, Schwanninger M, Rodrigues J (2012) A common near infrared-based partial least squares regression model for the prediction of wood density of *Pinus pinaster* and *Larix* x *eurolepis*. Wood Sci Technol 46: 157–175.

Anderegg WRL, Klein T, Bartlett M, Sack L, Pellegrini AFA, Choat B, Jansen S (2016) Meta-analysis reveals that hydraulic traits explain cross-species patterns of drought-induced tree mortality across the globe. Proc Natl Acad Sci USA 113:5024–5029.

Barigah T, Gyenge JE, Sergent AS et al. (2019) Application of pneumatic method to buildvulnerability curves in solitary vesseled trees: Assessement of vulnerability to cavitation of three Eucalyptus species. International Conference "Adapting forest ecosystems and wood products to biotic and abiotic stress", Bariloche, Argentina. March 12–15.

Barigah TS, Charrier O, Douris M, Bonhomme M, Herbette S, Améglio T, Fichot R, Brignolas F, Cochard H (2013) Water stress-induced xylem hydraulic failure is a causal factor of tree mortality in beech and poplar. Ann Bot 112:1431–1437.

Barigah TS, Gyenge JE, Barreto F, Rozenberg P, Fernández ME (2021) Narrow vessels cavitate first during a simulated drought in *Eucalyptus camaldulensis*. Physiol Plant 173:2081–2090.

Barotto AJ, Fernández ME, Gyenge J, Meyra A, Martínez-Meier A, Monteoliva S (2016) First insights into the functional role of vasicentric tracheids and parenchyma in *Eucalyptus* species with solitary vessels: Do they contribute to xylem efficiency or safety? Tree Physiol 36:1485–1497.

Barotto AJ, Monteoliva S, Gyenge J, Martínez-Meier A, Moreno K, Tesón N, Fernández ME (2017) Wood density and anatomy of three *Eucalyptus* species: implications for hydraulic conductivity. For Syst 26:e010 1–e010 11.

Barotto AJ, Monteoliva S, Gyenge J, Martínez-Meier A, Fernández ME (2018) Functional relationships between wood structure and vulnerability to xylem cavitation in races of *Eucalyptus globulus* differing in wood density. Tree Physiol 38:243–251.

Beć KB, Grabska J, Czarnecki MA (2018) Spectra-structure correlations in NIR region: spectroscopic and anharmonic DFT study of n-hexanol, cyclohexanol and phenol. Spectrochim Acta A Mol Biomol Spectrosc 197:176–184.

Booth TH (2013) Eucalypt plantations and climate change. For Ecol Manag 301:28–34.

Cappa EP, Pathauer PS, Lopez GA (2010) Provenance variation and genetic parameters of *Eucalyptus viminalis* in Argentina. Tree Genet Genomes 6:981–994.

Choat B, Brodribb TJ, Brodersen CR, Duursma RA, López R, Medlyn BE (2018) Triggers of tree mortality under drought. Nature 558:531–539.

Cochard H, Casella E, Mencuccini M (2007) Xylem vulnerability to cavitation varies among poplar and willow clones and correlates with yield. Tree Physiol 27:1761–1767.

Corcuera L, Cochard H, Gil-Pelegrin E, Notivol E (2011) Phenotypic plasticity in mesic populations of *Pinus pinaster* improves resistance to xylem embolism (P_{50}) under severe drought. Trees Struct Funct 25:1033–1042.

Costa FRC, Lang C, Almeida DRA, Castilho CV, Poorter L (2018) Near-infrared spectrometry allows fast and extensive predictions of functional traits from dry leaves and branches. Ecol Appl 28: 1157–1167.

Dalla-Salda G, Martínez-Meier A, Cochard H, Rozenberg P (2011) Genetic variation of xylem hydraulic properties shows that wood density is involved in adaptation to drought in Douglas-fir (*Pseudotsuga menziesii* (Mirb.)). Ann For Sci 68:747–757.

Fernández ME, Barotto AJ, Martínez Meier A et al. (2019) New insights into wood anatomy and function relationships: how *Eucalyptus* challenges what we already know. For Ecol Manag 454: 117638.

Greenwood S, Ruiz-Benito P, Martínez-Vilalta J et al. (2017) Tree mortality across biomes is promoted by drought intensity, lower wood density and higher specific leaf area. Ecol Lett 20:539–553.

Grossiord C, Sevanto S, Borrego I et al. (2017) Tree water dynamics in a drying and warming world. Plant Cell Environ 40: 1861–1873.

Gyenge JE, Fernández ME, Dalla Salda G, Schlichter T (2005) Leaf and whole-plant water relations of the Patagonian conifer *Austrocedrus chilensis* (D. Don) Pic. Ser. et Bizzarri: implications on its drought resistance capacity. Ann For Sci 62:297–302.

Hacke UG, Sperry JS (2001) Functional and ecological xylem anatomy. Perspectives in Plant Ecology, Evolution and Systematics 4(2): 97-115. https://doi.org/10.1078/1433-8319-00017

Hacke UG, Sperry JS, Wheeler JK, Castro L (2006) Scaling of angiosperm xylem structure with safety and efficiency. Tree Physiol 26:689–701.

Hacke UG, Jacobsen AL, Pratt RB (2009) Xylem function of arid-land shrubs from California, USA: an ecological and evolutionary analysis. Plant Cell Environ 32:1324–1333.

Hajek P, Link RM, Nock CA et al. (2022) Mutually inclusive mechanisms of drought-induced tree mortality. Glob Chang Biol 28:3365–3378.

Hein PRG (2012) Estimating shrinkage, microfibril angle and density of *Eucalyptus* wood using near infrared spectroscopy. J Near Infrared Spectrosc 20:427–436.

Inagaki T, Schwanninger M, Kato R, Kurata Y, Thanapase W, Puthson P, Tsuchikawa S (2012) *Eucalyptus camaldulensis* density and fiber length estimated by near-infrared spectroscopy. Wood Sci Technol 46:143–155.

InsideWood (2004–onwards) Published on the Internet. http://insidewood.lib.ncsu.edu/search (6 December 2022, date last accessed).

Jacobsen AL, Ewers FW, Pratt RB, Paddock WA III, Davis SD (2005) Do xylem fibers affect vessel cavitation resistance? Plant Physiol 139:546–556.

Jacquin P, Longuetaud F, Leban J-M, Mothe F (2017) X-ray microdensitometry of wood: a review of existing principles and devices. Dendrochronologia 42:42–50.

Jinagool W, Rattanawong R, Sangsing K, Barigah TS, Gay F, Cochard H, Kasemsap P, Herbette S (2015) Clonal variability for vulnerability to cavitation and other drought-related traits in Hevea brasiliensis Müll. Arg. Journal of Plant Hydraulics 2: e001. https://doi.org/10.20870/jph.2015.e001

Jones PD, Schimleck LR, Peter GF, Daniels RF, Clark A III (2005) Non-destructive estimation of *Pinus taeda* L tracheid morphological characteristics for samples from a wide range of sites in Georgia. Wood Sci Technol 39:529–545.

Lachenbruch B, Mcculloh KA (2014) Traits, properties, and performance: how woody plants combine hydraulic and mechanical functions in a cell, tissue, or whole plant. New Phytol 204:747–764.

Lamacque L, Charrier G, dos Santos FF, Lemaire B, Améglio T, Herbette S (2020) Drought-induced mortality: branch diameter variation reveals a point of no recovery in lavender species. Plant Physiol 183:1638–1649.

Lamy J-B, Delzon S, Bouche PS, Alia R, Vendramin GG, Cochard H, Plomion C (2014) Limited genetic variability and phenotypic plasticity detected for cavitation resistance in a Mediterranean pine. New Phytol 201:874–886.

Leblon B, Adedipe O, Hans G et al. (2013) A review of near-infrared spectroscopy for monitoring moisture content and density of solid wood. For Chron 89:595–606.

Li H, Liang Y, Xu Q, Cao D (2009) Key wavelengths screening using competitive adaptive reweighted sampling method for multivariate calibration. Anal Chim Acta 648:77–84.

Lobo A, Torres-Ruiz JM, Burlett R et al. (2018) Assessing inter- and intraspecific variability of xylem vulnerability to embolism in oaks. For Ecol Manag 424:53–61.

Lopez GA, Potts BM, Dutkowski GW, Rodriguez Traverso JM (2001) Quantitative genetics of *Eucalyptus globulus*: affinities of land race and native stand localities. Silvae Genetica 50:244–252.

López R, Cano FJ, Choat B, Cochard H, Gil L (2016) Plasticity in vulnerability to cavitation of *Pinus canariensis* occurs only at the driest end of an aridity gradient. Front Plant Sci 7:769.

Luss S, Schwanninger M, Rosner S (2015) Hydraulic traits of Norway spruce sapwood estimated by Fourier transform near-infrared spectroscopy (FT-NIR). Can J For Res 45:625–631.

Mannes D, Lehmann E, Cherubini P, Niemz P (2007) Neutron imaging versus standard X-ray densitometry as method to measure tree-ring wood density. Trees 21:605–612.

Mantova M, Menezes-Silva PE, Badel E, Cochard H, Torres-Ruiz JM (2021) The interplay of hydraulic failure and cell vitality explains tree capacity to recover from drought. Physiol Plant 172: 247–257.

Mevik B-H, Wehrens R (2007) The pls Package: principal component and partial least squares regression in R. J Stat Softw 18:1–23.

Minasny B, McBratney A (2013) Why you don't need to use RPD. Pedometron 33:14–15.

Ona T, Sonoda T, Ito K, Shibata M, Ootake Y, Ohshima J, Yokota S, Yoshizawa N (1999) Quantitative FT-Raman spectroscopy to measure wood cell dimensions. Analyst 124:1477–1480.

Ozaki Y (2012) Near-infrared spectroscopy - Its versatility in analytical chemistry. Anal Sci 28:545–563.

Peguero-Pina JJ, Sancho-Knapik D, Barrón E, Camarero JJ, Vilagrosa A, Gil-Pelegrín E (2014) Morphological and physiological divergences within *Quercus ilex* support the existence of different ecotypes depending on climatic dryness. Ann Bot 114: 301–313.

Polge H (1966) Établissement des courbes de variation de la densité du bois par exploration densitométrique de radiographies d'échantillons prélevés à la tarièresur des arbres vivants: applications dans les domaines Technologique et Physiologique. Annales des sciences forestières, INRA/EDP Sciences 23:I-206.

Pritzkow C, Williamson V, Szota C, Trouvé R, Arndt SK (2020) Phenotypic plasticity and genetic adaptation of functional traits influences intra-specific variation in hydraulic efficiency and safety. Tree Physiol 40:215–229.

Savi T, Tintner J, Sois LD, Grabner M, Petit G, Rosner S (2019) The potential of Mid-Infrared spectroscopy for prediction of wood density and vulnerability to embolism in woody angiosperms. Tree Physiol 39:503–510.

Savitzky A, Golay MJE (1964) Smoothing and differentiation of data by simplified least squares procedures. Anal Chem 36:1627–1639.

Schimleck LR, Evans R (2004) Estimation of *Pinus radiata* D. Don tracheid morphological characteristics by near infrared spectroscopy. Holzforschung 58:66–73.

Schimleck LR, Michell AJ, Raymond CA, Muneri A (1999) Estimation of basic density of *Eucalyptus globulus* using near-infrared spectroscopy. Can J For Res 29:194–201.

Schimleck LR, Mora C, Daniels RF (2004) Estimation of tracheid morphological characteristics of green *Pinus taeda* L. radial strips by near infrared spectroscopy. Wood Fiber Sci 36:527–535.

Schwanninger M, Rodrigues JC, Fackler K (2011) A review of band assignments in near infrared spectra of wood and wood components. J Near Infrared Spectrosc 19:287–308.

Sergent AS, Segura V, Charpentier JP, Dalla-Salda G, Fernández ME, Rozenberg P, Martínez-Meier A (2020) Assessment of resistance to xylem cavitation in cordilleran cypress using near-infrared spectroscopy. For Ecol Manag 462:117943.

Serra-Maluquer X, Gazol A, Anderegg WRL, Martínez-Vilalta J, Mencuccini M, Camarero JJ (2022) Wood density and hydraulic traits influence species' growth response to drought across biomes. Glob Chang Biol 28:3871–3882.

Shukla S, Shashikala S, Sujatha M (2021) Non-destructive estimation of fibre morphological parameters and chemical constituents of *Tectona grandis* L.f. wood by near infrared spectroscopy. J Near Infrared Spectrosc 29:168–178.

Signal Developers (2014) signal: Signal processing. http://r-forge.r-project.org/projects/signal/ (6 December 2022, date last accessed).

Sperry JS, Donnelly JR, Tyree MT (1988) A method for measuring hydraulic conductivity and embolism in xylem. Plant Cell Environ 11:35–40.

Tsuchikawa S, Kobori H (2015) A review of recent application of near infrared spectroscopy to wood science and technology. J Wood Sci 61:213–220.

Urli M, Porté AJ, Cochard H, Guengant Y, Burlett R, Delzon S (2013) Xylem embolism threshold for catastrophic hydraulic failure in angiosperm trees. Tree Physiol 33:672–683.

Viana LC, Trugilho PF, Hein PRG, Lima JT, da Silva JRM (2009) Predicting the morphological characteristics and basic density of *Eucalyptus* wood using the NIRS technique. Cerne 15:421–429.

Wold S (1978) Cross-validatory estimation of the number of components in factor and principal components models. Dent Tech 20: 397–405.

Wortemann R, Herbette S, Barigah TS, Fumanal B, Alia R, Ducousso A, Gomory D, Roeckel-Drevet P, Cochard H (2011) Genotypic variability and phenotypic plasticity of cavitation resistance in *Fagus sylvatica* L. across Europe. Tree Physiol 31: 1175–1182.

Ziemińska K, Butler DW, Gleason SM, Wright IJ, Westoby M (2013) Fibre wall and lumen fractions drive wood density variation across 24 Australian angiosperms. AoB PLANTS 5: 1–14.